Available online at www.sciencedirect.com
SCIENCE DIRECT®
Journal of Sound and Vibration 288 (2005) 701–728
JOURNAL OF SOUND AND VIBRATION
www.elsevier.com/locate/jsvi

Numerical and experimental validation of variance prediction in the statistical energy analysis of built-up systems

V. Cotoni[a,*], R.S. Langley[b], M.R.F. Kidner[c]

[a]*ESI US R&D Inc., 12555 High Bluff Drive, Suite 250, San Diego, CA 92130, USA*
[b]*Department of Engineering, University of Cambridge, Trumpington Street, Cambridge CB2 1PZ, UK*
[c]*Vibration and Acoustics Laboratory, Virginia Polytechnic Institute and State University, Blacksburg, VA 24061, USA*

Accepted 5 July 2005
Available online 31 August 2005

Abstract

In the statistical energy analysis (SEA) approach to vibration modeling, a complex system is represented as an assembly of coupled subsystems, and the method leads to the prediction of the vibrational energy level of each subsystem. The averaging procedures implicit in the technique imply that the predicted energy is the mean value taken over an ensemble of random structures, such as a set of vehicles leaving a production line. Recently, a new method has been developed to allow the ensemble variance, in addition to the mean, to be predicted within the context of SEA, and the present paper concerns further extension and validation of this work. The theoretical extension concerns the variance of the energy density at a single point in any of the subsystems, and the validation includes both simulation and experimental studies. The simulation results concern plate assemblies, while experimental results are presented both for a single-plate and for a cylinder-plate structure. In each case an ensemble of random structures has been generated by adding small point masses at random locations on the structure. In general, good agreement between the predictions and the validation results is observed.

*Corresponding author. Tel.: +1 858 350 0057; fax: +1 858 350 8328.
E-mail address: vincent.cotoni@esi-group-na.com (V. Cotoni).

0022-460X/$ - see front matter © 2005 Elsevier Ltd. All rights reserved.
doi:10.1016/j.jsv.2005.07.012

1. Introduction

The prediction of the high-frequency response of a complex dynamic system is a difficult task for two reasons. Firstly, the deformation of the system is of short wavelength, which means that very many degrees of freedom are required to model the response in detail, and secondly the response is sensitive to small changes in the properties of the system. The second point can lead to nominally identical items from the same production line having very different behavior, as clearly demonstrated for automotive structures by the experimental results of Bernhard and Kompella [1]. Both of these difficulties are addressed by statistical energy analysis (SEA) [2], where an energy flow model is used in place of a detailed deterministic model of the system. The degrees of freedom are the vibrational and acoustic energy levels of various regions, or subsystems, of the structure. Relatively few subsystems are employed, typically tens or hundreds, which is several orders of magnitude less than the number of degrees of freedom required in a detailed deterministic model, thus avoiding the first difficulty. The second difficulty is addressed by certain averaging procedures which are implicit in SEA, and which imply that the computed energy levels represent ensemble mean values—for example, the mean interior noise level in a fleet of vehicles from a production line. There has been recent progress in extending SEA to the prediction of the variance of the subsystem energies [3], and the present paper is concerned with the further extension and validation of this work.

The prediction of the variance of the vibrational energy of a single isolated subsystem has been the subject of research for many years. In early work it was assumed that the natural frequencies of the subsystem form a Poisson point process [4], but more recently this has been extended to the case of natural frequencies governed by the Gaussian orthogonal ensemble (GOE) [5]. There is much numerical and experimental evidence that real systems conform to the GOE [6–8], and single subsystem predictions based on this assumption have shown good agreement with simulations [9,10]: one key difference between Poisson and GOE natural frequencies lies in the statistical distribution of the spacings between successive natural frequencies. Under the Poisson assumption this distribution is exponential, whereas the GOE assumption yields a Rayleigh distribution. The latter is more consistent with the veering phenomenon that occurs in complex systems without special symmetries—a full discussion of this issue can be found in Refs. [6–8].

There has also been much interest in the statistics of the response of built-up systems [2], and recently the single subsystem GOE analysis has been extended to a general assembly of subsystems [3]. This allows the variance of the subsystems energies to be computed as a simple post-processing stage to a standard SEA analysis. The aim of the present work is two-fold: (i) to extend the theory of Ref. [3] to the variance of the energy density at a single point in any of the subsystems, and (ii) to provide numerical and experimental validation of the theory. The first aim is motivated by the fact that practical interest is often focused on a single response point—for example, the sound level at the driver's ear, rather than the total sound level in the interior of a vehicle. The second aim is to add to the range of validation studies presented in Ref. [3], by considering ensembles of structures both via simulation and via experiment. The simulation results concern plate assemblies, while the experimental results concern both a single-plate and a cylinder-plate assembly. In all cases, a random ensemble has been generated by adding small masses at random locations on the structure.

It should be noted that in the literature there are two approaches to analyzing variance within the context of SEA that are quite different from both a philosophical and a practical point of view. The present approach, and that of Refs. [2,3], aims to compute the variance of the system energy levels across an ensemble of random structures. Within this approach, it is recognized that the standard SEA equations govern the ensemble mean energies, and that these equations are not necessarily valid for a single member of the ensemble. The other approach is to randomize the various coefficients that appear in the SEA equations (for example, the coupling loss factors), and then calculate the statistics of the energy levels yielded by these equations [11,12]. In effect, this second approach considers the variance of the ensemble mean energy across an "ensemble of ensembles", when there are gross changes to the system properties (junction lengths, subsystem areas, etc.) across the top-level ensemble. This approach would yield zero variance for all of the examples considered here, where there are no gross changes to the system properties. If the system properties *are* subject to gross changes, then the present approach can be viewed as yielding conditional values of the mean and variance, and Bayes theorem can be used to incorporate the effect of the large-scale uncertainties.

SEA and the variance prediction theory are summarized in Section 2, and the extension of the theory to the energy density at a point is given in Section 3. Numerical validation results are then presented in Section 4, and experimental results are reported in Section 5.

2. SEA and energy variance prediction

2.1. General equations

In the SEA approach to vibration prediction, an engineering system is represented as an assembly of coupled subsystems, and one aim is to find the vibrational energy E_j for each subsystem j. The approach is based on the principle of power balance, and the governing equation for the jth subsystem at vibration frequency ω is [2]

$$\omega\eta_j E_j + \sum_k \omega\eta_{jk} n_j (E_j/n_j - E_k/n_k) = P_{\mathrm{in},j}. \tag{1}$$

Here η_j is the loss factor of subsystem j, n_j is the modal density of the subsystem, $P_{\mathrm{in},j}$ is the power input from external sources, and η_{jk} is the coupling loss factor from subsystem j to subsystem k. SEA is concerned with systems that are inherently random, such as items from a production line, where the response may be sensitive to relatively small manufacturing variabilities. The subsystem energies E_j yielded by the method are the *ensemble average* energies, where the ensemble consists of the population of random structures. Likewise, $P_{\mathrm{in},j}$ represents the ensemble average power input; for ease of notation, and to conform with standard SEA usage, the expectation symbol E[ ] is not written explicitly for these quantities, i.e. more strictly the terms should be written as E[E_j] and E[$P_{\mathrm{in},j}$]. The energy may be further averaged over a frequency band, in which case the frequency ω that appears in Eq. (1) represents the center frequency of the band. Eq. (1) can be re-expressed in matrix form as

$$\mathbf{C}\hat{\mathbf{E}} = \mathbf{P}_{\mathrm{in}}, \tag{2}$$

where $\hat{E}_j = E_j/n_j$ is the ensemble mean 'modal energy' of subsystem j, and the entries of the matrix $\mathbf{C}$ and the vector $\mathbf{P}_{\text{in}}$ follow immediately from Eq. (1). Strictly, following the argument above Eq. (2), $\hat{E}_j$ should be written as $\mathrm{E}[\hat{E}_j]$ to emphasize the fact that Eq. (2) governs the ensemble-averaged modal energy; however, the more standard notation is retained here.

Eq. (1) has recently been extended to the prediction of the ensemble variance of the subsystem energies [3]. An equation in the form of Eq. (2) can actually be written for each member of the random ensemble of systems, with all three terms taken to be random across the ensemble, and with the energy vector representing the energy of the *particular member* system, rather than the ensemble average energy. A perturbation expansion of this equation, taken around the mean values, can then be performed. It follows that to the first order in the random perturbations, the SEA matrix $\mathbf{C}$ is equal to the ensemble average of the random matrix. To the same order, an expression can be obtained for the random part of the modal energies that is linear in the random part of the matrix and in the random part of the power input, $\mathbf{C}_{\text{ran}}$ and $\mathbf{P}_{\text{ran}}$ say. This then leads to the result

$$\mathrm{Var}[\hat{E}_j] = \sum_k (C_{jk}^{-1})^2 \mathrm{Var}[P_{\text{ran},k}] + \sum_k \sum_{s\neq k} \left\{ (C_{jk}^{-1} - C_{js}^{-1})\hat{E}_s \right\}^2 \mathrm{Var}[C_{\text{ran},ks}], \tag{3}$$

where $\mathrm{Var}[\hat{E}_j]$ represents the ensemble variance of the modal energy in the jth subsystem, and C_{jk}^{-1} represents the jk entry of the inverse of the SEA matrix $\mathbf{C}$. Here again, the term $\hat{E}_s$ in the second sum should strictly be written as $\mathrm{E}[\hat{E}_s]$, as it represents the ensemble averaged modal energy in the sth subsystem. Two important issues in the derivation of Eq. (3) are: (i) the matrix $\mathbf{C}_{\text{ran}}$ is not necessarily symmetric, even though the mean SEA matrix $\mathbf{C}$ *is* symmetric, and (ii) the entries of the matrix $\mathbf{C}_{\text{ran}}$ are not uncorrelated, as a result of the energy balance condition that applies to any member system. It is shown in Ref. [3] that

$$\mathrm{Var}[P_{\text{ran},k}] = P_{\text{in},k}^2 r^2(\alpha_k, m'_k, B'_k), \quad \mathrm{Var}[C_{\text{ran},ks}] = C_{ks}^2 r^2(\alpha_{ks}, m'_k, B'_k), \tag{4,5}$$

where

$$\eta'_k = 1/(\omega n_k C_{kk}^{-1}), \quad m'_k = \omega \eta'_k n_k, \quad B'_k = \Delta/(\omega \eta'_k). \tag{6,7,8}$$

The term η'_k is the in-situ loss factor for subsystem k [2], m'_k is the half-power modal overlap factor arising from this loss factor, and B'_k is a bandwidth parameter which represents the number of modal bandwidths within the frequency-averaging band Δ ($B'_k = 0$ if no frequency averaging is considered). The function r^2 that appears in Eqs. (4) and (5) is given by [9,10]

$$r^2(\alpha, m, B) \approx \frac{\alpha - 1}{\pi m B^2}\left\{2B \tan^{-1} B - \ln(1 + B^2)\right\} + \frac{\ln(1 + B^2)}{(\pi m B)^2}. \tag{9}$$

This result is actually an approximation that becomes increasingly accurate with increasing m. For $B = 0$, an alternative result is available that is accurate for all values of m [9]

$$r^2(\alpha, m, 0) = \frac{1}{\pi m}\left\{\alpha - 1 + \frac{1}{2\pi m}\left[1 - \mathrm{e}^{-2\pi m}\right] + \mathrm{E}_1(\pi m)\left[\cosh(\pi m) - \frac{1}{\pi m}\sinh(\pi m)\right]\right\}, \tag{10}$$

where E_1 is the exponential integral. The assumptions and approximations that underlie Eqs. (3)–(10) are fully discussed in Ref. [3], but it is worth noting that the key assumptions underpinning the method are: (i) SEA provides a good estimate of the mean subsystem energies,

so that the normal requirements of SEA (for example weak coupling) are met; (ii) each subsystem is sufficiently random to exhibit statistical overlap, so that GOE statistics apply to the natural frequencies. The only "non-SEA" parameters that appear in these equations are the terms α_k and α_{ks} in Eqs. (4) and (5), which are discussed in the following section.

2.2. The parameters α_k and α_{ks}

The key result that underpins the variance theory summarized in the previous section concerns the statistics of the response of a single uncoupled subsystem. Regardless of the form of the excitation, the reverberant energy of one particular realization of the subsystem can be written as twice the kinetic energy, in the form of a modal expansion [9,10]

$$E = \frac{\omega^2}{2} \sum_n \int_{\omega-\Delta/2}^{\omega+\Delta/2} \frac{a_n}{(\omega_n^2 - \omega^2)^2 + (\eta\omega_n^2)^2} \, \mathrm{d}\omega, \tag{11}$$

where the sum is taken over the modes of the subsystem, and a_n is the modulus squared generalized force associated with the nth mass-normalized mode. The relative variance of E has been shown to be [9,10]

$$\frac{\mathrm{Var}[E]}{\mathrm{E}[E]^2} = r^2(\alpha, m, B), \tag{12}$$

where r^2 is the function given by Eq. (9) or Eq. (10), and m and B are, respectively, the modal overlap and bandwidth parameters, as given by Eqs. (7) and (8), with the symbols interpreted appropriately for the special case of a single subsystem. The parameter α is defined as

$$\alpha = \frac{\mathrm{E}[a_n^2]}{\mathrm{E}[a_n]^2}. \tag{13}$$

Eq. (12) is based on the assumption that the statistics of the subsystem natural frequencies conform to the GOE. Justification for this is given in Refs. [9,10], but it is worth noting here that the assumption requires "statistical overlap", i.e. the system must be sufficiently random for the standard deviation of random shifts in a particular natural frequency across the ensemble to exceed half the mean frequency spacing. This condition is likely to be met at higher frequencies where the modal spacing is small relative to any particular natural frequency, but is less likely to be met at low frequencies, where the subsystem behavior can be near deterministic [3].

Eq. (4) of the general variance theory is built upon the assumption that subsystem k is weakly coupled to other subsystems, so that the external power input to subsystem k can be written in the form of Eq. (11), and the relative variance equation, Eq. (12), can be applied to give the relative variance of the power input. The parameter α_k therefore depends upon the nature of the power input, via Eq. (13). If the power arises from a force $f(\mathbf{x})$ distributed over the domain Ω of the subsystem, then a_n is written as

$$a_n = \left| \int_\Omega f(\mathbf{x}) \phi_n(\mathbf{x}) \, \mathrm{d}\mathbf{x} \right|^2, \tag{14}$$

where ϕ_n is the nth mode shape of subsystem k. The value of α_k will thus depend on the nature of $f(\mathbf{x})$ and the statistics of the subsystem mode shapes. In the case of a spatially random force (for

example, a turbulent boundary layer), the energy may be pre-averaged over the force statistics for each member of the random ensemble of structures. In this case, Eq. (14) becomes

$$a_n = \left\langle \left| \int_\Omega f(\mathbf{x})\phi_n(\mathbf{x})\,\mathrm{d}\mathbf{x} \right|^2 \right\rangle = \iint_{\Omega,\Omega} \left\langle f(\mathbf{x})f^*(\mathbf{x}') \right\rangle \phi_n(\mathbf{x})\phi_n(\mathbf{x}')\mathrm{d}\mathbf{x}\,\mathrm{d}\mathbf{x}', \tag{15}$$

where $\langle\ \rangle$ represents an average over the force statistics.

Eq. (5) of the general variance theory is also based on the single subsystem analysis: as discussed in Ref. [3], the response of subsystem k to excitation arising at the boundary with subsystem s could be treated the same way as external forces, using Eq. (11). The coefficient $C_{\mathrm{ran},ks}$ can be interpreted as the power input to subsystem k when subsystem s has a *prescribed* energy of unity, and hence the analysis concerns the dynamic properties of subsystem k alone, rather than the coupled dynamics of both subsystems. In this case, Eq. (14) is again appropriate, with $f(\mathbf{x})$ interpreted as the force applied by subsystem s, and the domain Ω interpreted as the interface between the two subsystems: the fact that subsystem s has a prescribed energy of unity implies that $f(\mathbf{x})$ can be treated in exactly the same way as an external force of prescribed amplitude. The term α_{ks} then follows from Eq. (13), and the resulting value will depend on the nature of the coupling between the subsystems and the statistics of the mode shapes. If the system response is pre-averaged over any spatially random external forces, then an equation analogous to Eq. (15) will apply for the coupling forces, since on any given member of the ensemble the coupling forces will vary with each realization of the external loading.

Given Eqs. (13) and (14,15), it might be thought that the calculation of α_k and α_{ks} will be a daunting task for a complex system. This is not the case however, and a compendium of values has been derived for a wide range of power inputs and subsystem couplings [13]. To take one example, consider two subsystems that are coupled along an extended junction (i.e. not at several discrete points). From the central limit theorem, the generalized force arising from subsystem s can be expected to approach a complex Gaussian random process, in which case a_n in Eq. (14) will have an exponential distribution. It then follows from Eq. (13) that $\alpha_{ks} = 2$. This simple result will apply to many types of practical junction. Other results for α_k and α_{ks} that are relevant to the examples considered in Sections 4 and 5 are given in Appendix A.

3. The variance of energy density at a point in a subsystem

The analysis given in the previous sections allows the variance of the total energy in a subsystem to be computed. In some cases there may also be interest in the statistics of the response at a particular point in a subsystem. This response can be written as

$$u(\mathbf{x}) = \sum_n \frac{G_n\phi_n(\mathbf{x})}{\omega_n^2(1+\mathrm{i}\eta)-\omega^2}, \quad G_n = \int_\Omega f(\mathbf{x}')\phi_n(\mathbf{x}')\,\mathrm{d}\mathbf{x}', \tag{16,17}$$

where, as in Eq. (14), $f(\mathbf{x})$ is the applied force, which may arise from external forces and from other subsystems. The resonant energy density at the point $\mathbf{x}$ is proportional to the modulus squared response; for the purposes of the present analysis the constant of proportionality can be

omitted, and the energy density can be written as

$$\varepsilon(\mathbf{x}) = \left|u(\mathbf{x})\right|^2. \tag{18}$$

An approximate result for the relative variance of ε can be derived by considering a heuristic argument based on conditional probability. If the total energy of the subsystem is known deterministically to be E then $u(\mathbf{x})$ may vary randomly over the subsystem, but it must satisfy the relation

$$\int_A \varepsilon(\mathbf{x})\,\mathrm{d}\mathbf{x} = E \Rightarrow \langle \varepsilon(\mathbf{x}) \rangle = E/A, \tag{19}$$

where A represents the total length, area or volume of the subsystem, and $\langle\ \rangle$ consequently represents the spatial average. It is now assumed, based on the central limit theorem, that the spatial statistics of u have a complex Gaussian distribution; this is analogous to the approach to room acoustics taken by Schroeder [14]. It then follows that ε has an exponential distribution, for which the relative variance is unity, so that

$$\langle \varepsilon(\mathbf{x})^2 \rangle = 2(E/A)^2. \tag{20}$$

Now Eqs. (19) and (20) represent the *conditional* mean and mean squared value of ε for a specified value of E. If E is now taken to be random across the ensemble, with mean value $\mathrm{E}[E]$ and relative variance r_E^2, then the unconditional statistical moments of ε can be found by averaging Eqs. (19) and (20) over the ensemble to give

$$\mathrm{E}[\varepsilon] = \mathrm{E}[E]/A, \quad \mathrm{E}[\varepsilon^2] = 2(r_E^2 + 1)\mathrm{E}[E]^2/A^2. \tag{21,22}$$

The relative variance of ε is then given by

$$r_\varepsilon^2 = 1 + 2r_E^2. \tag{23}$$

Thus, if the relative variance of the subsystem energy is given by the analysis of Section 2, then the relative variance of the energy density at a point can be estimated from Eq. (23).

The analysis leading to Eq. (23) is far from rigorous, and it is therefore advisable to seek supporting evidence from the existing literature. Burkhard and Weaver [6] and Lobkis et al. [15] have derived the statistics of the Green's function of a single subsystem, based on the assumption of GOE natural frequency statistics. This analysis can be applied to Eqs. (16) and (18) by making several minor changes to the notation, and it follows that the relative variance of ε is given by

$$r_\varepsilon^2 = 1 + \frac{1}{\pi m}\left\{\frac{\mathrm{E}\left[|G_n|^4\right]\mathrm{E}\left[\phi_n^4\right]}{\mathrm{E}\left[|G_n|^2\right]^2\mathrm{E}\left[\phi_n^2\right]^2} - g(\pi m)\right\}. \tag{24}$$

The function g is detailed in Ref. [15], and ranges from $g = 0$ at low modal overlap ($m = 0$) to $g = 3$ at high modal overlap ($m = \infty$). In the same notation, the relative variance of the total subsystem energy is given to first order in $1/\pi m$ by [6,9]

$$r_E^2 = \frac{1}{\pi m}\left\{\frac{\mathrm{E}\left[|G_n|^4\right]}{\mathrm{E}\left[|G_n|^2\right]^2} - 1\right\}. \tag{25}$$

As the modal overlap factor increases, the function g asymptotes to 3, and Eqs. (24) and (25) then support the general form of Eq. (23). In this case, rather than having the fixed value 2, the coefficient of the second term will depend upon both the statistics of the mode shapes and the statistics of the loading. For Gaussian mode shapes, the modal ratio that appears in Eq. (24) would have the value 3, although numerical simulations of various random systems have shown that the mode shapes have a slightly negative excess of kurtosis [15,16], and a closer approximation is 2.7. With this value, it follows that

$$r_\varepsilon^2 = 1 + \left(\frac{2.7\beta - 3}{\beta - 1}\right) r_E^2, \tag{26}$$

where the value of β is determined by the statistics of the generalized force. For a point load ($\beta = 2.7$) the corresponding result would be $r_\varepsilon^2 = 1 + 2.52 r_E^2$, while for a complex Gaussian generalized force ($\beta = 2$) the result is $r_\varepsilon^2 = 1 + 2.4 r_E^2$. A more deterministic load, with say $\beta = 1.25$, would yield $r_\varepsilon^2 = 1 + 1.5 r_E^2$. For comparison, were the natural frequencies assumed to be Poisson, rather than GOE, then the result for point loading would be $r_\varepsilon^2 = 1 + 2.25 r_E^2$ [4]. This result further supports the general form of Eq. (23), although there is some variation in the coefficient of the second term. The coefficient of 2 suggested by Eq. (23) can be viewed as a tentative value requiring validation against benchmark studies, and such studies are reported in Sections 4 and 5.

Thus far, the effect of frequency band averaging on the energy density has not been considered. In the case of Poisson natural frequencies, Lyon [4] has shown for a single subsystem that both r_ε^2 and r_E^2 are scaled by a function $F(B)$, where B is the bandwidth parameter defined by Eq. (8) and

$$F(B) = \frac{2}{B} \tan^{-1}(B) - \frac{1}{B^2} \ln(1 + B^2). \tag{27}$$

In the case of GOE statistics, the first two terms in Eq. (24) are also scaled by $F(B)$, but the modification to the term involving g is much more complex. In view of this behavior, a suitable empirical modification to Eq. (23) to allow for the effect of band averaging is

$$r_\varepsilon^2 = F(B) + 2 r_E^2, \tag{28}$$

where r_E^2 is now the result for the band-averaged total energy. At very high modal overlap, Eq. (28) yields $r_\varepsilon^2 \approx F(B)$, which is in agreement with a result obtained by Schroeder [17].

Another case of interest concerns the variance of the energy density when the system is subjected to spatially random loading, such as rain-on-the-roof. Here the principle of reciprocity can be applied: the energy density at a point in subsystem k caused by rain-on-the-roof loading in subsystem s is proportional to the total energy in subsystem s caused by point loading in subsystem k. The relative variance relating to the latter problem is given by the theory presented in Section 2, and hence a solution to the former problem can be found.

4. Comparison with numerical simulations

Numerous computational validation studies relating to the variance theory presented in Section 2 have been given in Ref. [3]. This section describes an additional validation case, which is directed primarily at the new material regarding the energy density at a point presented in Section 3. The

validation case also serves to highlight key differences between the present variance formulation and the earlier variance theory of Ref. [2]. The method reported in Ref. [2] provides many insights into variance propagation through a built-up structure, but it is based on Poisson natural frequency statistics rather than the present GOE approach, and there are detailed differences from the current theory that are summarized in Appendix B.

4.1. The system considered: two edge-connected plates

The example considered consists of two coupled plates, the properties of which are given in Table 1. The plates are coupled along a common edge, and to emphasize the differences between the variance formulations presented in Refs. [2,3], the parameters are chosen to give very different values of modal overlap in the two plates. Plate 1 is excited by a harmonic transverse point force, and only the bending motion is considered (i.e. in-plane motion is not included). Both plates are rectangular and simply supported, with rotational compatibility along the common edge, and the construction material is aluminum (Young's modulus $7.2 \times 10^{10}\,\mathrm{N/m^2}$, density $2800\,\mathrm{kg/m^3}$, and Poisson's ratio 0.3).

Benchmark Monte Carlo simulation results have been obtained by using the Lagrange–Rayleigh–Ritz method with the sine–sine mode shapes of the uncoupled plates as basis functions. Randomization of each plate has been achieved by adding ten point masses at random locations, with each mass having 2% of the total mass of the plate, and three rotational springs randomly located on each edge (except the edge common to both plates). The added masses and springs are accounted for in the analysis by adding the appropriate kinetic and potential energies to the Lagrangian. The coupling condition along the common edge was enforced by adding stiff rotational springs to ensure rotational compatibility. An ensemble of 100 systems has been generated and solved. The choice of rectangular plates has been made here as an analytical convenience. Although a rectangular geometry with simply supported boundary conditions has certain special symmetry properties (due to the fact that the system can be represented as a set of uncoupled waveguides), these properties are destroyed by the addition of random masses and springs. Thus, the present results would be expected to be reproduced for plates of different geometry having the same gross properties (area, junction length, etc.) as the present plates.

4.2. Statistics of the plate energies

4.2.1. Energy due to a single deterministic point force

For the case of a single deterministic point load applied to plate 1, the energies of the two plates are shown in Fig. 1 as functions of frequency for each of the 100 generated samples. The ensemble

Table 1
Properties of the two-plate structure

Plate	Thickness (mm)	Size (m × m)	Loss factor η (%)	Modal density (modes/Hz)	Modal overlap m at 700 Hz
1	1	1.05×1.30	5	0.445	15.5
2	5	1.25×1.30	0.02	0.106	0.015

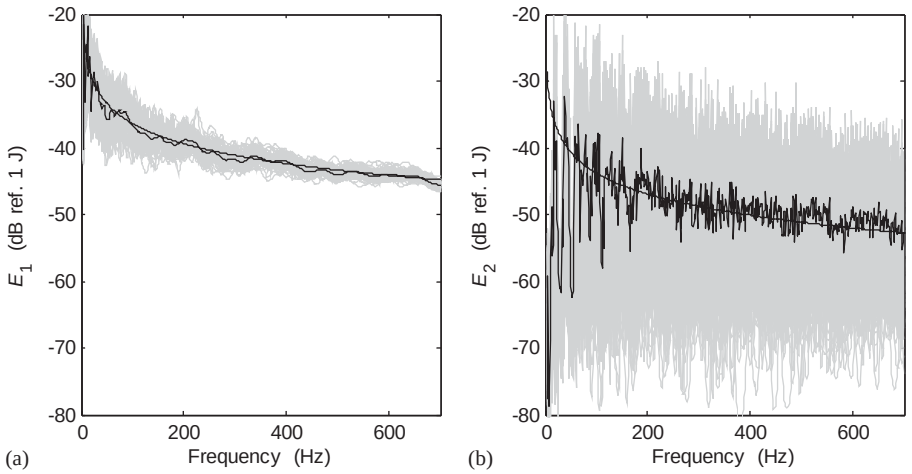

Fig. 1. Energy frequency response of two line-connected random plates, when plate 1 is driven by a point force. (a) plate 1; (b) plate 2. Gray: energy response of each sample; fluctuating black: mean response over all samples; smooth black: SEA prediction.

mean values are also shown. It can be seen that the mean energy is lower in plate 2 than in plate 1, while the scatter in the energy (related to the variance) is much higher. The frequency range covers approximately 311 resonant modes of plate 1 and 74 resonant modes of plate 2. The mean energy predictions from SEA are also shown in the figure, and these show good agreement with the Monte Carlo results. It can be noted that the mean energies as given by the Monte Carlo simulation are not entirely smooth functions of frequency, and this can be traced primarily to the limited sample size employed in the present analysis. As in all the following figures, the simulation (or experimental) results are fluctuating curves and the theoretical predictions are smooth curves.

Theoretical predictions for the relative variance are compared with the simulation results in Fig. 2. Results from the theory presented in Ref. [2] are plotted with dashed lines, while results from Eq. (3) are plotted with solid lines. When applying the variance theory from Ref. [2], the following parameters have been employed (the equation numbers refer to those given in Ref. [2]): Eq. (12.3.4) yields $\alpha_k = (3/2)^2$ for point force loading, while Eq. (12.3.7) yields $\alpha_k = \alpha_s = 3/2$ for a line coupling between the plates. For the present variance theory, Eq. (A.2) of Appendix A yields $\alpha_1 = 2.7$ for use in Eq. (4), and Eq. (A.6) yields $\alpha_{12} = \alpha_{21} = 2$ for use in Eq. (5).

Some details of the differences between the two variance formulations are given in Appendix B. Because the coupling between the plates is fairly weak, the variance of the driven plate is primarily due to the variance of the input power from the point load. The slight overestimation of the variance of plate 1 by the theory of Ref. [2] is mainly related to the first point listed in Appendix B regarding Eq. (B.1), i.e. it arises from the consideration of Poisson rather than GOE natural frequency statistics (see Ref. [9] for a more detailed discussion). The GOE results show closer agreement with the simulations, as also found in previous studies [3,9]. The underestimation of the variance of plate 2 by the theory of Ref. [2] can be explained with reference to Eq. (B.2) of Appendix B. The very high modal overlap of plate 1 yields a very small variance for the coupling term as given by Ref. [2], Eq. (B.2a); in contrast, Eq. (B.2b) of the present theory yields a much

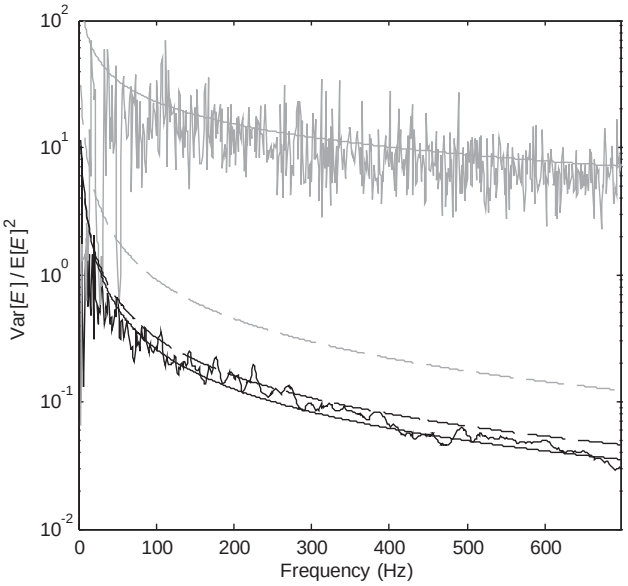

Fig. 2. Relative variance of the energy of two line-connected random plates, as a function of frequency, when plate 1 is driven by a point force. Black: plate 1; gray: plate 2. The predictions from the current formulation are plotted with solid lines. The predictions based on Ref. [2] are plotted with dashed lines.

larger variance that depends upon the modal overlap of plate 2 alone. The results shown in Fig. 2 help to justify the assumptions made in Ref. [3] regarding the non-symmetric structure of the random part of the energy-power matrix, leading to Eq. (B.2b).

The results for the plate energies when averaged over 12th-octave-frequency bands (which gives a bandwidth of approximately 40 Hz at 700 Hz) are shown in Fig. 3. While the mean energies are virtually unchanged by band averaging, the relative variance is slightly reduced for plate 1 and much more reduced for plate 2, and this is reasonably well predicted by employing Eq. (9) rather than Eq. (10) in the variance theory. It can be noted that for 12th-octave-bands the bandwidth parameter in Eq. (9) is $B'_k = (2^{1/24} - 2^{-1/24})/\eta'_k$, where η'_k is the in-situ loss factor for subsystem k. The fact that the loss factor is relatively high for plate 1 implies that the bandwidth parameter is small, and hence the relative variance is not much affected by band-averaging; conversely, the loss factor for plate 2 is low, leading to a large bandwidth parameter and a large reduction in the relative variance. For example, values at 700 Hz are $B'_1 \sim 1.2$, and $B'_2 \sim 52.5$.

4.2.2. Energy due to pre-averaged forcing: rain-on-the-roof

If plate 1 is subjected to spatially random rain-on-the-roof forcing, then the concern is with the power spectrum of the response, and this requires pre-averaging the response over different realizations of the forcing before considering variations across the ensemble of random structures [3]. For rain-on-the-roof forcing, this pre-averaging has the same effect as averaging over the location of a single deterministic point load. Theoretical predictions for the relative variance under rain-on-the-roof forcing are compared with simulation results in Fig. 4, where good

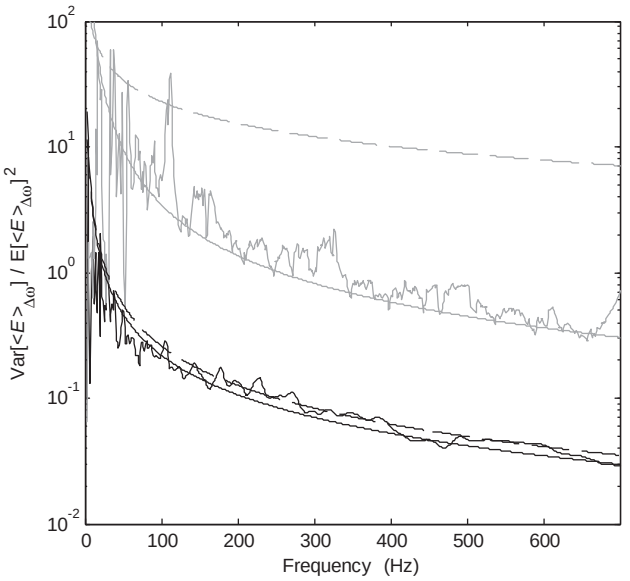

Fig. 3. Relative variance of the 1/12 octave-band-averaged energy of two line-connected random plates, as a function of frequency, when plate 1 is driven by a point force. Black: plate 1; gray: plate 2. The predictions from the current formulation are plotted with solid lines. The predictions from Fig. 2 for pure-tone responses are plotted with dashed lines.

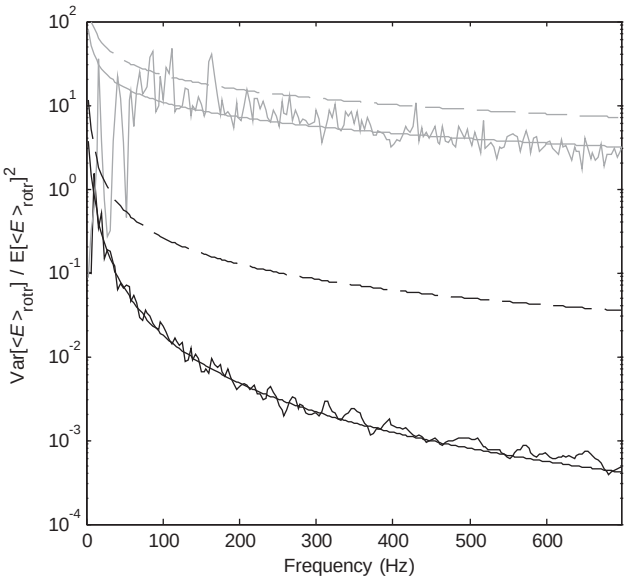

Fig. 4. Relative variance of the pre-averaged energy of two line-connected random plates, as a function of frequency, when plate 1 is driven by rain-on-the-roof forcing. Black: plate 1; gray: plate 2. Predictions are plotted with solid lines. The predictions from Fig. 2 for a point force (i.e. without pre-averaging) are plotted with dashed lines.

agreement is demonstrated. In this case, Eq. (3) was employed with $\alpha_1 = 1$ in accordance with Eq. (A.3), and $\alpha_{12} = \alpha_{21} = 1$ in accordance with Eq. (A.7). The results for a deterministic point force are also shown in the figure for comparison. It can be seen that the relative variance of the driven plate is much smaller for rain-on-the-roof loading than for a deterministic point force, while the relative variance of plate 2 is less significantly reduced. The reason why the energy variances are not similarly altered can be explained by considering Eq. (10): when $\alpha = 1$ the first term involving $1/\pi m$ vanishes, leaving only the term involving $1/(\pi m)^2$. The effective modal overlap of plate 1 is large ($m_1' \sim 15.5$ at 700 Hz), making a difference of the order $r^2(2.7, m_1', 0)/r^2(1, m_1', 0) \sim 85.7$ between single-point ($\alpha_1 = 2.7$) and rain-on-the-roof ($\alpha_1 = 1$) forcing. In contrast, for plate 2 ($m_2' \sim 0.08$ at 700 Hz) the corresponding change arising from α_{21} is much less, with $r^2(2.7, m_2', 0)/r^2(1, m_2', 0) \sim 3.1$.

4.3. Statistics of the energy density at a point

The statistics of the modulus squared displacement at one point on each plate has been computed from both the Monte Carlo simulations and the SEA and variance equations. The observation points were chosen to be remote from the driving point and from the plate edges to avoid near-field and correlation effects that are not covered by SEA and the present variance theory. The mean modulus squared displacement can be predicted from the SEA mean energy $\mathrm{E}[E]$ by using the relation $\mathrm{E}[|u(\mathbf{x}, \omega)|^2] = 2\mathrm{E}[E(\omega)]/M\omega^2$, where M is the mass of the plate. When single point loading is applied to the system, the relative variance of the modulus squared displacement (or energy density) is given by Eq. (23). The theoretical predictions are compared with the Monte Carlo simulations in Fig. 5, where good agreement is demonstrated. For

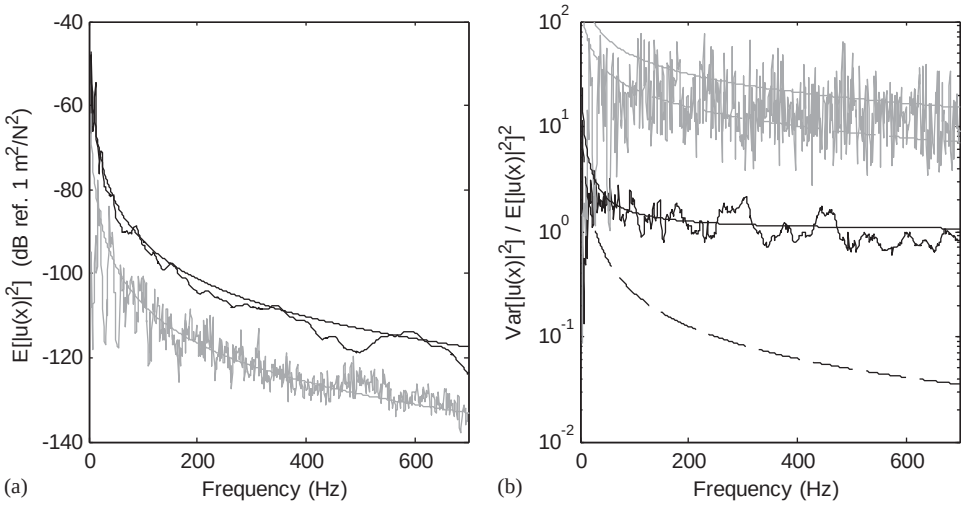

Fig. 5. Ensemble mean and variance of the modulus squared displacement at a point, as a function of frequency, for two line-connected random plates with plate 1 driven by a point force. (a) Mean; (b) relative variance. Black: point in plate 1; gray: point in plate 2. Fluctuating curves: Monte Carlo results; smooth solid lines: predictions; smooth dashed lines: predictions from Fig. 2 for energy responses (instead of energy density).

comparison, results relating to the total energies of each plate are also shown in the figure: the relative variance of the energy density at a point is shown to be much higher than the relative variance of the total energy (especially for the driven plate).

Results for the 12th-octave-band averaged energy density are shown in Fig. 6. In this case, Eq. (28) gives the relative variance of the energy density in terms of the relative variance of the total energy in each plate, which is in turn given by Eq. (3) in conjunction with Eq. (9). Reasonable agreement between simulations and predictions can be seen in Fig. 6, although the relative variance for the energy density in plate 2 is slightly underestimated. The prediction for pure-tone data is also shown for comparison. It can be seen that the effect of frequency averaging is much more noticeable for plate 2 than for plate 1, as already observed and explained for the total energy.

If plate 1 is subjected to spatially random rain-on-the-roof forcing, then the response is pre-averaged over different realizations of the forcing before considering variations across the ensemble of random structures. As discussed at the end of Section 3, the relative variance of the response at a point under rain-on-the-roof forcing is the same as the relative variance of the energy under single-point forcing in the reciprocal problem. Theoretical predictions for the relative variance under rain-on-the-roof forcing are compared with simulation results in Fig. 7, where good agreement is demonstrated. The results for a deterministic point force are also shown in the figure for comparison. The behavior noticed for the total energy is also observed here, in that changing the point forcing to rain-on-the-roof forcing reduces the relative variance on the driven plate much more than the relative variance on plate 2. This feature is captured by the theory.

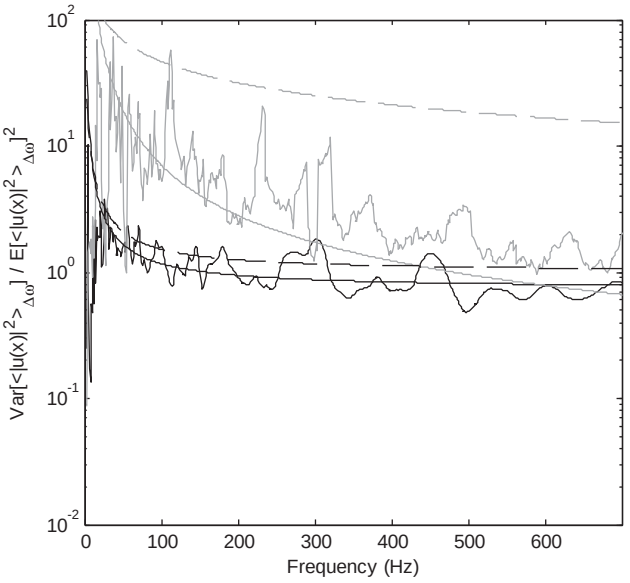

Fig. 6. Relative variance of the 1/12 octave-band-averaged modulus squared displacement at a point, as a function of frequency, for two line-connected random plates with plate 1 driven by a point force. Black: point in plate 1; gray: point in plate 2. Fluctuating curves: Monte Carlo results; smooth solid lines: predictions. Smooth dashed lines: predictions from Fig. 5 for pure-tone responses.

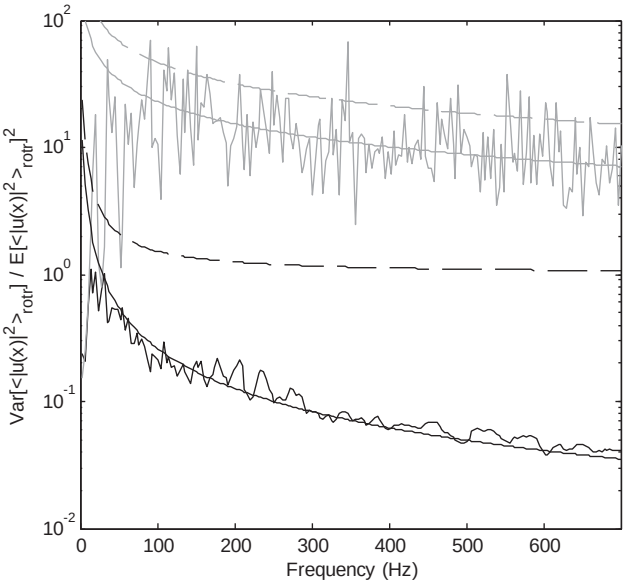

Fig. 7. Relative variance of the modulus squared displacement at a point, as a function of frequency, for two line-connected random plates with plate 1 driven by rain-on-the-roof forcing. Black: point in plate 1; gray: point in plate 2. Fluctuating curves: Monte Carlo results; smooth solid lines: predictions. Smooth dashed lines: predictions from Fig. 5 for loading by a point force (i.e. without pre-averaging).

5. Comparison with experimental results

5.1. A single plate

5.1.1. The test structure and the experimental setup

Experimental validation studies have been performed on the steel plate shown in Fig. 8. Viscoelastic damping patches of irregular shape were glued to the plate to increase the loss factor, which was estimated by measuring the input power P_{in} and flexural energy E (assuming this is equal to twice the kinetic energy) and by applying the power balance equation $P_{\text{in}} = \eta\omega E$. The result was found to be approximately constant over the frequency range of interest, and is given together with the other properties of the plate in Table 2. The plate was randomized by adding a set of nine masses at random locations. A total of 19 configurations were tested over the frequency range 25 to 1250 Hz, and only out-of-plane motion was considered. The plate was excited at five fixed locations by an impact hammer equipped with a force sensor, and the transverse acceleration was measured, with accelerometers at the excitation point and at 12 other points scattered over the plate. The complex force–displacement transfer functions were computed from the acceleration–force cross-spectra S_{A_kF}, and the force auto-spectrum S_{FF}, by using the relation $u(\mathbf{x}_k, \omega) = -S_{A_kF}(\omega)/\omega^2 S_{FF}(\omega)$. The time-averaged flexural energy of the plate was deduced from the total mass M and the measured data by using $E(\omega) = \langle |S_{A_kF}(\omega)/S_{FF}(\omega)|^2 \rangle_k M/2\omega^2$, where $\langle\ \rangle_k$ denotes an average over the accelerometers. Finally, the input power was estimated from

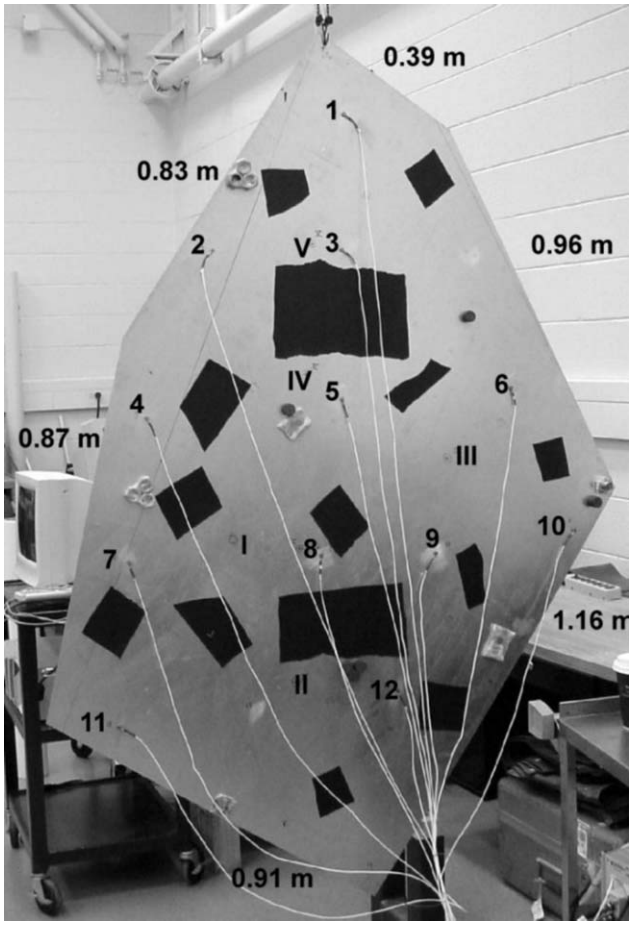

Fig. 8. Experimental setup for the single plate. The Roman numerals indicate the five excitation points, the Arabic numerals indicate the 12 observation points. The added masses are taped or magnetically attached to the plate. The black patches are the damping treatment.

Table 2
Properties of the experimental plate

Material (steel)	Dimensions	Damping factor η	Mass	Added mass
$E = 2.1 \times 10^{11}\,\mathrm{N\,m^{-2}}$, $v = 0.3$, $\rho = 7800\,\mathrm{kg\,m^{-1}}$	S$\sim$2 m^2, $h = 1$ mm	1.39%	15.6 kg	1.6 kg ($\sim$10%)

$P_{\mathrm{in}}(\omega) = \mathrm{Im}\{S_{A_0F}(\omega)/S_{FF}(\omega)\}/2\omega$ where S_{A_0F} is the acceleration-force cross-spectrum for the accelerometer at the loading point.

5.1.2. *Statistics of the total energy*

Two examples of measured energy responses are shown in Fig. 9: the response to a single point force is shown in Fig. 9(a), while the response averaged over five forcing locations is shown in

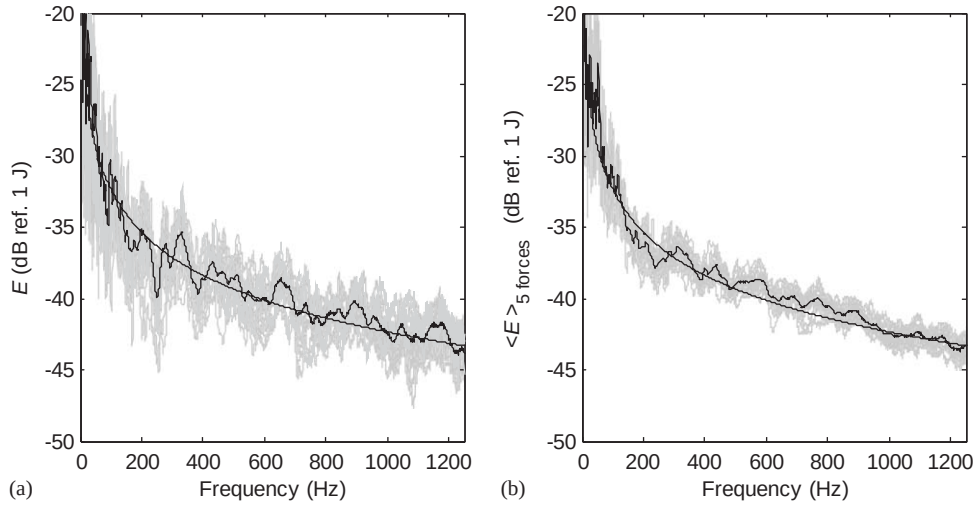

Fig. 9. Energy of the random plate as a function of frequency. (a) Energy with one point load; (b) energy averaged over five point loads. Gray: response of each experimental sample; fluctuating black: mean response over all 19 samples; smooth line: SEA prediction.

Fig. 9(b). In each diagram, the gray lines are the response curves for each of the 19 samples, the fluctuating black line is the ensemble mean, and the smooth black line is the SEA prediction given by $\mathrm{E}[E(\omega)] = P_{\mathrm{in}}^{\infty}/\eta\omega$, where $P_{\mathrm{in}}^{\infty} = 1/16(D\rho h)^{1/2}$ is the power input to an infinite plate of flexural rigidity D. The SEA prediction is the same for both loading cases, and good agreement is found with the measured data. The corresponding relative variances of the energy are shown in Fig. 10. The theoretical predictions shown in the figure have been made by using Eq. (3) with $\alpha_1 = K$ for the single-point load, as given by Eq. (A.2), and $\alpha_1 = 1 + (K-1)/5$ for the average over five-point loads, as given by Eq. (A.3), with K taken to be 2.7. The modal overlap factor ($m_1 = n\eta\omega$) required in Eq. (4) was obtained from the measured damping and the theoretical modal density of the plate, given by $n = S(\rho h/D)^{1/2}/4\pi$ ($n \approx 0.1\ \mathrm{Hz}^{-1}$). The modal overlap factor is a linear function of frequency, with a value of approximately 8.8 at 1000 Hz. It can be seen from Fig. 10 that the relative variance is much reduced when the energy is averaged over the five excitation points, and this is well predicted by the theory.

The energy responses have been averaged over moving frequency bands of width $\Delta = 10\eta\omega$. The ensemble mean of the energy is almost unaffected by the averaging process, but the variance is reduced, as shown in Fig. 11. The theoretical predictions shown in this figure have been made by using Eq. (9) with $B = 10$. The experimental variance has a fairly erratic behavior, due in part to the relatively small ensemble considered here, but the average trends are reasonably well predicted by the theory.

5.1.3. *Statistics of the energy density at a point*

The mean and relative variance of the modulus squared transfer function between two fixed points on the plate are shown in Fig. 12. The SEA prediction of the mean value follows from the predicted mean energy via $\mathrm{E}[|u(\mathbf{x}_k, \omega)|^2] = 2\mathrm{E}[E(\omega)]/M\omega^2$. The prediction of the relative variance

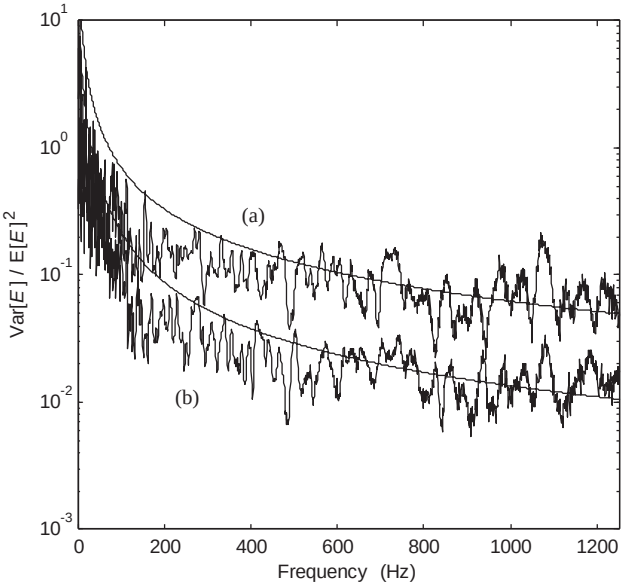

Fig. 10. Relative variance of the pure-tone energy of the single plate versus frequency. (a) Energy with one point force; (b) energy averaged over five point forces. The predictions are the smooth lines.

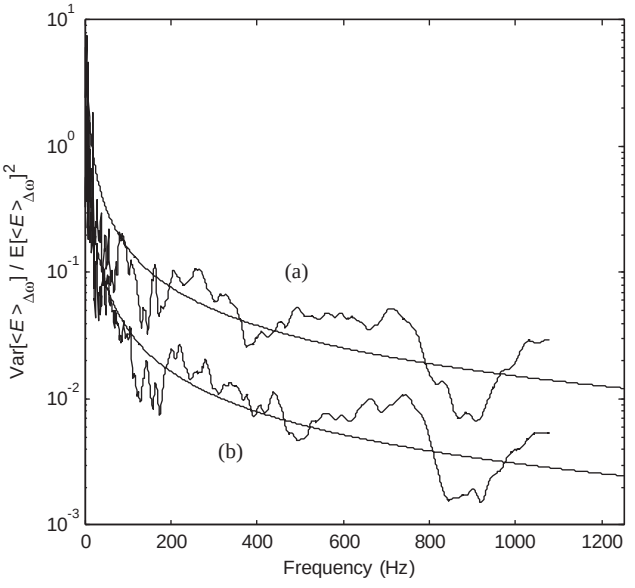

Fig. 11. Relative variance of the frequency-band-averaged energy of the single plate versus frequency ($\Delta = 10\,\eta\omega$). (a) Energy with one point force; (b) energy averaged over five point forces. The predictions are the smooth lines.

follows from Eq. (23). While the predicted mean agrees fairly well with the experimental results, the relative variance is over-predicted. Surprisingly, the experimental results yield a relative variance that is less than unity at some frequencies, whereas the theory implies that the result

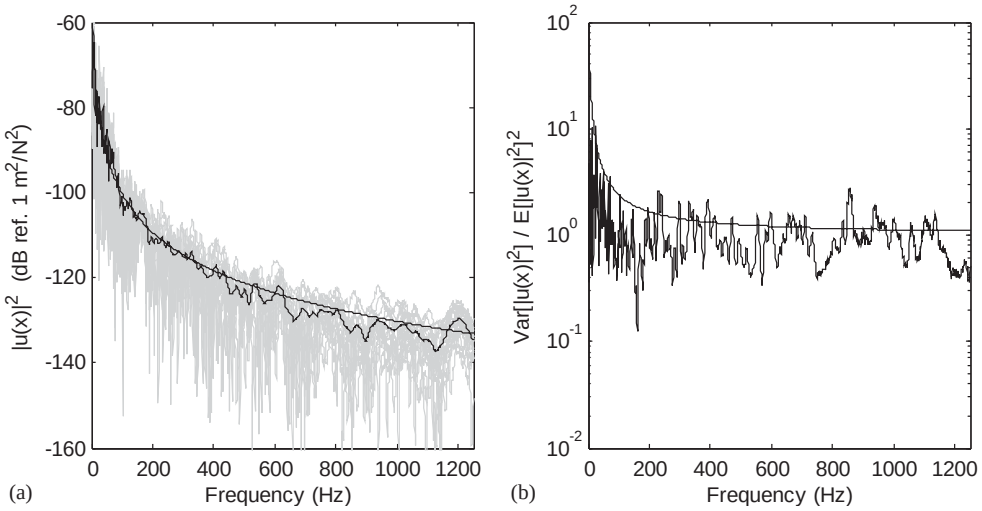

Fig. 12. (a) Modulus squared of the displacement frequency transfer function between two points. Gray: response of each experimental sample; fluctuating black: mean response over all 19 samples; smooth line: SEA prediction. (b) Relative variance of modulus squared displacement as a function of frequency. Fluctuating curve: experimental results; smooth line: prediction.

should always exceed unity (unity is the lower limiting value, obtained for very large modal overlap where Schroeder statistics apply [14]). Two potential causes of this discrepancy have been investigated: (i) it is possible that the direct field due to the point force produces a significant deterministic component of response across the ensemble, which reduces the relative variance, and (ii) perhaps the 19 experimental samples are insufficient to yield a converged result for the relative variance. Point (i) was found not to have a significant effect for the current system, since the direct field is much less than the reverberant field. Point (ii) was investigated by performing Monte Carlo simulations for a system having the same gross parameters as the experimental structure, and the results obtained are shown in Fig. 13. With 19 samples (black curve) the results are similar to those found in the experiment, while for 200 samples (gray curve) the relative variance is higher and in much closer agreement with the theoretical result. Without being a rigorous investigation, this suggests that the discrepancies shown in Fig. 12 are due to a lack of convergence in the experimental ensemble. A system that is resonant at the excitation frequency and has a high value of the relevant mode shape at both the drive and response points will exhibit a very large response. Such systems occur rarely in the ensemble, but will have a large influence on the variance of the response; thus, the considered ensemble must be large enough to capture a sufficient number of these systems.

5.2. A cylinder with three attached plates

5.2.1. The test structure and the experimental setup

The structure shown in Fig. 14 comprises three plates connected to a circular bracket attached at one end of a cylinder. The plates are identical in terms of material, thickness, damping

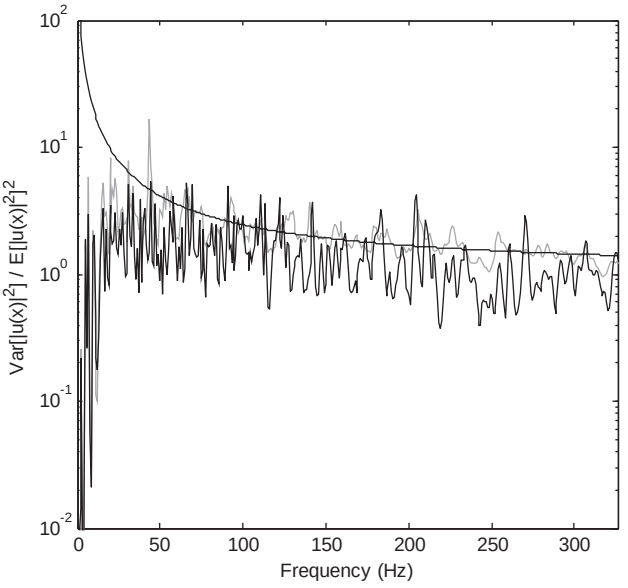

Fig. 13. Relative variance of modulus squared displacement as a function of frequency. Fluctuating black: Monte Carlo simulation with 19 samples; fluctuating gray: Monte Carlo simulation with 200 samples; smooth line: prediction.

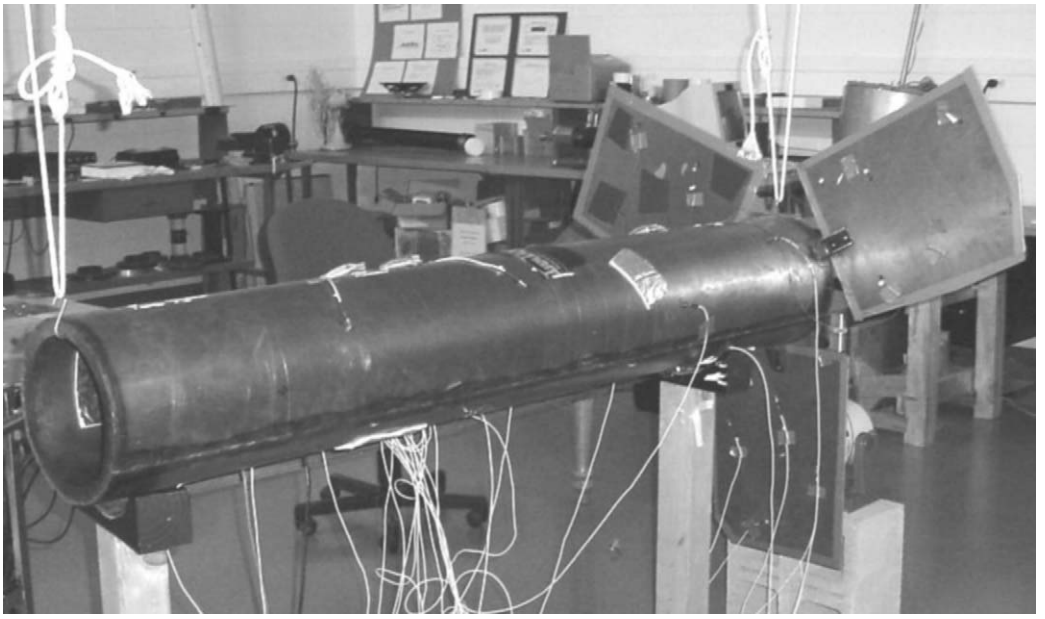

Fig. 14. Cylinder-plate structure and experimental setup; the figure shows with the lower plate driven by a point force (shaker).

Table 3
Properties of the cylinder and attached plates

	Dimensions	Damping factor α (%)	Mass (kg)	Total added masses
Plates	$a\sim0.4$ m, $b\sim0.5$ m, $h=1$ mm	1.5	1.5	340 kg (22%)
Cylinder	$r=0.14$ m, $l=1.83$ m, $h=1$ mm	0.6	13.6	3.6 kg (26%)

treatment and area, whereas the exact geometries differ. All components are of steel, with the properties given in Table 2 (aside from the loss factor), and other properties of the system are given in Table 3. The loss factors shown in Table 3 were measured by the power injection method, with viscoelastic damping material glued to the structure, and they were found to be approximately independent of frequency. An ensemble of random systems was generated by attaching masses at random locations on each substructure. Four masses were attached to each plate and ten masses to the cylinder, and the total amount of mass used is shown in Table 3.

The assembled structure was suspended at two points as shown in Fig. 14. The experimental setup consisted of one shaker, one impedance head at the excitation point, ten accelerometers scattered on the cylinder, and four accelerometers scattered on each plate. A white noise signal was applied to the shaker, which was attached either to one of the plates or to the cylinder. Valid data were obtained up to 5000 Hz in the first case, and up to 7500 Hz in the second case (limitations arise from the signal to noise ratio). Respectively, 25 and 30 samples were tested for these configurations.

5.2.2. Statistics of the subsystem energies

An SEA model of the system was built within the software package AutoSEA [18] by describing the connections between the plates and the cylinder as point junctions, since for much of the frequency range the bending wavelength in the cylinder and plates is much longer than the bracket dimensions (0.04 m). The mean input power used in the SEA model was based on the relevant theoretical result for an infinite system, with a mass correction factor accounting for the presence of the impedance head: $\mathrm{E}[P_{\mathrm{in}}] = P_{\mathrm{in}}^{\infty}/|1 + \mathrm{i}2M_a P_{\mathrm{in}}^{\infty}|^2$, where M_a is the mass of the device between the force sensor and the subsystem (estimated at 4.5 g), and P_{in}^{∞} is the infinite subsystem power input per unit force. The mass effect of the impedance head was found to be significant (more than 10 dB at 5000 Hz).

The variance of the energy in each subsystem is given by Eq. (3). The appropriate values of the α parameters are: $\alpha_k = K$ (point load, Eq. (A.2)), and $\alpha_{ks} = 2K$ (single-point junction, Eq. (A.4)), where K was taken to be 2.7. The modal overlap factors at 1000 Hz (based on the identified damping loss factors and theoretical modal densities) are 0.95 for the plates and 1.2 for the cylinder. These values increase respectively to 4.7 and 22.4 at 5000 Hz.

The experimental and predicted mean energies for loading on the cylinder are shown in Fig. 15(a). The SEA prediction can be seen to be satisfactory. The inflexion point in the curves at 5000 Hz corresponds to the ring frequency of the cylinder, below which the input power increases with frequency, and beyond which the input power is approximately constant with frequency. Since the configuration is symmetrical for the three plates, all three should have the same mean energy, and this is found both theoretically and experimentally. The relative variances of the

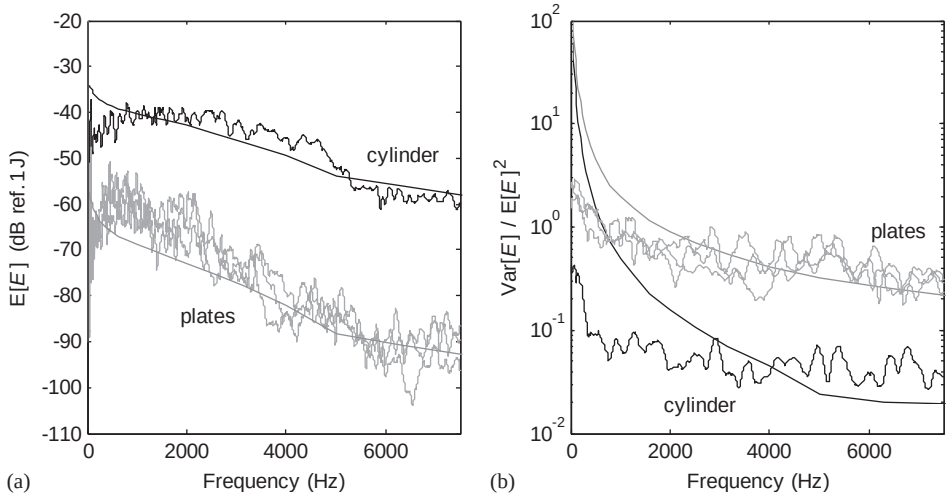

Fig. 15. Ensemble mean and variance of the energy frequency response of the cylinder and plates, when the cylinder is driven by a point force. (a) Mean; (b) relative variance. All three plates have similar responses. The predictions are the smooth lines.

energy are shown in Fig. 15(b). For clarity of presentation, the experimental relative variance curves have been smoothed by averaging over moving frequency bands of 200 Hz widths. Again, due to symmetry, the results are the same for each of the three plates. The prediction is far from exact, but captures the main trend. The relative variance of the cylinder is noticeably overpredicted at low frequencies. This is thought to be due, in part, to a lack of statistical overlap, i.e. the added masses are insufficient to completely randomize the cylinder at low frequencies, and thus the system is more deterministic than predicted by the theory.

The results obtained with forcing on plate 1 are shown in Fig. 16. The mean energies are reasonably well predicted by SEA, although the energies of plates 2 and 3 are underestimated. Due to symmetry, plates 2 and 3 should have the same mean response, and this is found to be the case in both the experimental and theoretical results. The relative variance predictions shown in Fig. 16(b) are a good approximation for all subsystems above 2000 Hz. Again, the relative variance is overpredicted at low frequencies, possibly due to insufficient randomization in the experimental arrangement.

As an example of the complete set of experimental data, the energy of each subsystem for each sample is shown in Fig. 17 for the case of a point load applied to plate 1. The gray curves are the responses for each sample; the fluctuating black curves are the means over all 30 samples. The same vertical scale is used for all diagrams, and it can be seen that the mean energy decreases from the driven plate 1, to the cylinder (which is the first connected subsystem), and to plates 2 and 3 (which are more "remote" from the driven subsystem). It can also be seen that the variance of the energy follows the opposite trend, with more scatter of the gray curves about the mean for plates 2 and 3 than for the cylinder and plate 1. The mean energies predicted by SEA are the smooth solid lines, and the 99% confidence bounds based on the predicted relative variance are plotted with dashed lines. These bounds were computed by assuming that the energy has a lognormal

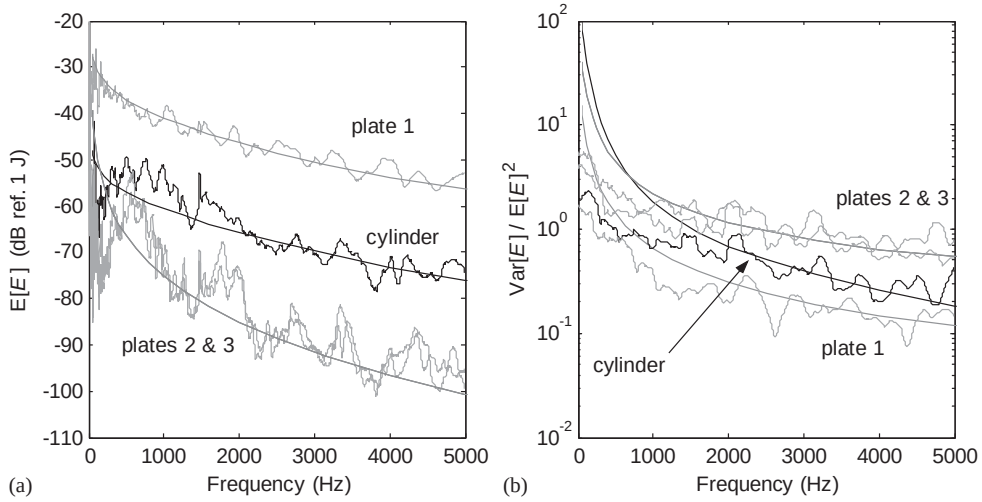

Fig. 16. Ensemble mean and variance of the energy frequency response of the cylinder and plates, when the plate 1 is driven by a point force. (a) Mean; (b) relative variance. The predictions are the smooth lines.

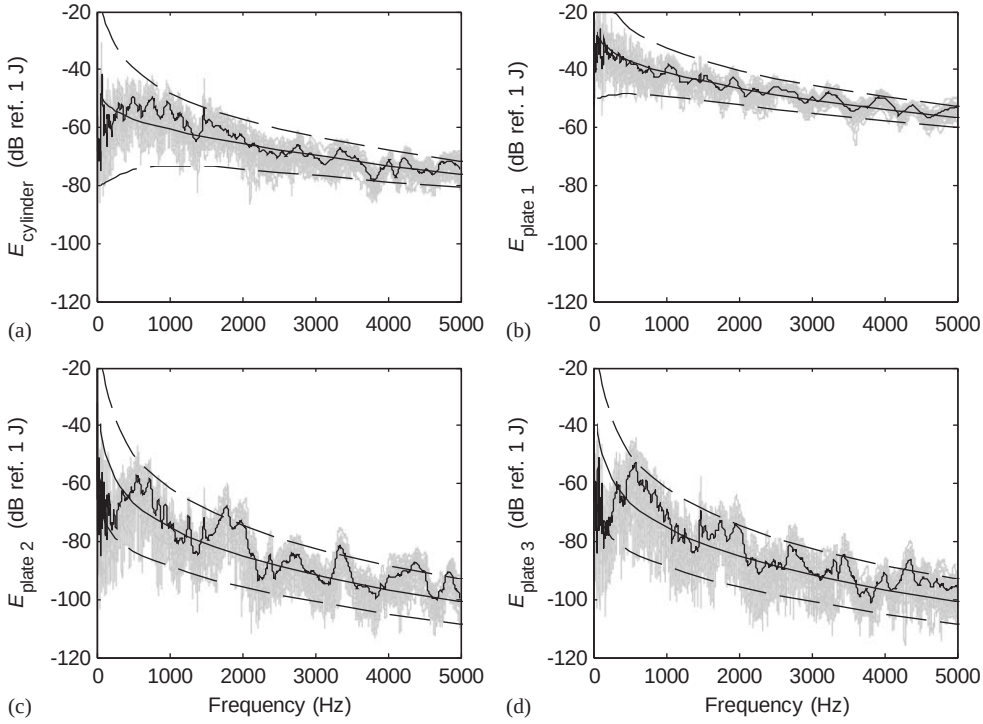

Fig. 17. Energy frequency response of the cylinder (a) and plates (b–d), when the plate 1 is driven by a point force. Gray: all 30 samples; fluctuating black: mean over the samples; smooth solid line: SEA prediction of the mean; dashed lines: bounds of the 99% confidence interval.

distribution, as suggested in the literature [2,19,20]. The details of this computation are given in Appendix C. The bounds define a fairly robust interval for the driven plate and cylinder, whose mean energy was shown to be well predicted by SEA. For the two remote plates, the experimental mean energy is not so well predicted by SEA, and this partly explains the poorer performance of the confidence bounds. As discussed in Ref. [3], the variance theory is based on the assumption that SEA yields a good estimate of the mean energy, and the theory is not designed to correct any bias in the predicted mean. In principle, the SEA model could have been updated to predict a closer approximation to the experimental mean prior to applying the variance theory, but this has not been performed as part of the present work.

6. Conclusions

The present paper has extended the analysis of Ref. [3] to the prediction of the variance of the energy density at a point within a built-up system. Numerical and experimental benchmark studies have been performed, with the aim of validating both the original theory and the new developments. In all cases the theory has been found to capture the qualitative trends of the benchmark results, with very good quantitative agreement in many cases. For the experimental data, it was found that the deviation from the predicted results is due in part to the limited number of samples in the experimental Monte Carlo ensemble.

The range of problems addressed in this paper covers the variance prediction of both total energy and energy density responses, either at a pure tone or averaged over frequency bands, for built-up systems subjected to deterministic point or spatially random rain-on-the-roof forcing. It should be emphasized that the present theory is based on SEA, and the only additional parameters required are the terms α_k and α_{ks} that are described in Section 2.2 and Appendix A. The method therefore shares the advantages and disadvantages of SEA: the main advantage is that the method is computationally efficient and easy to apply; the main disadvantage is that the conditions required for the successful application of SEA must be met.

Acknowledgments

This work was sponsored by the Air Force Research Laboratory, Space Vehicles Directorate, Kirtland AFB, NM, USA under SBIR Phase II contract F29601-02-C-0109. Helpful discussions with Phil Shorter and Bryce Gardner are also gratefully acknowledged.

Appendix A. The parameters α_k and α_{ks}

In this section, the values of the parameter α are given for a line coupling, a point coupling, and a point load. According to Eq. [13], the parameter α is defined as

$$\alpha = \frac{\mathrm{E}[a_n^2]}{\mathrm{E}[a_n]^2}, \tag{A.1}$$

where a_n is related to the modal force f_n applied by the loading or coupling on the nth mode shape of the subsystem. If one realization of force distribution is considered for each member of the ensemble of random systems, then a_n is given by Eq. (14). Alternatively, if an averaged is performed over several realizations of the force for each member of the ensemble, then a_n is given by Eq. (15).

A.1. α_k for a point load

For a deterministic point force of complex amplitude F acting at a location $\mathbf{x}$, Eq. (14) reduces to $a_n = |F|^2\phi_n^2(\mathbf{x})$. Substituting this result into Eq. (A.1) yields

$$\alpha_k = \frac{\mathrm{E}[\phi_n^2(\mathbf{x})]}{\mathrm{E}[\phi_n(\mathbf{x})]^2} = K. \tag{A.2}$$

It is assumed that K is independent of the location $\mathbf{x}$, and the appropriate value would be 3 for Gaussian mode shapes, and $(3/2)^d$ for sinusoidal mode shapes in system of dimension d [2,4]. It is suggested in the literature that the actual value for two-dimensional systems is around 2.7 [9,15].

Now, if a pre-average is performed over N random locations of the point force, then Eq. (15) becomes $a_n = |F|^2(1/N)\sum_k \phi_n(\mathbf{x}_k)^2$. This yields $\mathrm{E}[a_n] = |F|^2\mathrm{E}[\phi_n^2]$, and $\mathrm{E}[a_n^2] = |F|^4\ (\mathrm{E}[\phi_n^4]/N + \mathrm{E}[\phi_n^2]^2(N-1)/N)$, with the consequence that

$$\alpha_k = 1 + \frac{(K-1)}{N}. \tag{A.3}$$

For large N this type of load is equivalent to spatially random rain-on-the-roof, as often encountered in SEA, in which case $\alpha_k = 1$.

A.2. α_{ks} for a point coupling

Consider two subsystems s and k connected at N points. The N coupling forces are expected to have a random complex amplitude. As discussed in Ref. [3], if the forces are assumed to be uncorrelated and complex Gaussian, on the basis of Ref. [14], then for all forces F_i and F_j, one has $\mathrm{E}[|F_i|^2] = \mathrm{E}[|F_j|^2]$, $\mathrm{E}[|F_i|^4]/\mathrm{E}[|F_i|^2]^2 = 2$, $\mathrm{E}[F_iF_{j\neq i}^*] = 0$, and $\mathrm{E}[F_iF_j] = 0$.

For the case with one force configuration per member of the ensemble, Eq. (14) yields $a_n = |\sum_i F_i\phi_n(\mathbf{x}_i)|^2$. Assuming that the mode shapes and coupling forces are uncorrelated [3], it is found that $\mathrm{E}[a_n] = \sum_i \mathrm{E}[|F_i|^2]\mathrm{E}[\phi_n^2]$, and $\mathrm{E}[a_n^2] = \sum_i \mathrm{E}[|F_i|^4]\mathrm{E}[\phi_n^4] + 2\sum_{j\neq i}\mathrm{E}[|F_i|^2]\mathrm{E}[|F_j|^2]\mathrm{E}[\phi_n^2]^2$, which leads to

$$\alpha_{ks} = 2 + \frac{(2K-2)}{N}. \tag{A.4}$$

Now, if an average is performed over the coupling forces, Eq. (15) can be written as $a_n = \sum_i\sum_j \langle F_iF_j^*\rangle\phi_n(\mathbf{x}_i)\phi_n(\mathbf{x}_j)$, which according to the force cross-correlation properties can be rewritten as $a_n = \sum_i \langle|F_i|^2\rangle\phi_n^2(\mathbf{x}_i)$. This in turn yields $\mathrm{E}[a_n] = N\langle|F_i|^2\rangle\mathrm{E}[\phi_n^2]$

and $\mathrm{E}[a_n^2] = N\langle|F_i|^2\rangle^2\mathrm{E}[\phi_n^4] + (N-1)N\langle|F_i|^2\rangle^2\mathrm{E}[\phi_n^2]^2$, with the consequence that

$$\alpha_{ks} = 1 + \frac{(K-1)}{N}. \tag{A.5}$$

A.3. α_{ks} for a line coupling

For a subsystem k with a connection to a subsystem s along a line L, the generalized modal force arising from the junction can be written as $f_n = \int_L f(\mathbf{x})\phi_n(\mathbf{x})\,\mathrm{d}\mathbf{x}$, where f is the coupling force distribution along the line. If the correlation length of the integrand is short, then the generalized modal force is analogous to a summation of independent random variables, and from the central limit theorem it can be expected to approach a complex Gaussian random process. In the case of one force configuration per member of the ensemble, a_n is given by $|f_n|^2$ (Eq. (14)), and Eq. (A.1) then yields

$$\alpha_{ks} = 2. \tag{A.6}$$

This result is consistent with Eq. (A.4) when the number of coupling points N tends to infinity (continuous distribution of coupling forces).

Now, if a pre-average is performed over the coupling force distribution, then Eq. (15) becomes $a_n = \iint_{L,L'}\langle f(\mathbf{x})f^*(\mathbf{x}')\rangle\phi_n(\mathbf{x})\phi_n(\mathbf{x}')\,\mathrm{d}\mathbf{x}\,\mathrm{d}\mathbf{x}'$, where the function $\langle f(\mathbf{x})f^*(\mathbf{x}')\rangle$ is a deterministic quantity. If the correlation length of the mode shapes is short compared to the size of the junction, then the law of large numbers suggests that a_n will approach a deterministic value. In this case

$$\alpha_{ks} = 1, \tag{A.7}$$

which is consistent with Eq. (A.5) when the number of coupling points N tends to infinity.

Appendix B. A comparison between two variance theories

The major differences between the variance formulation proposed by Lyon and DeJong [2], and the one presented in this paper (with more details in Ref. [3]) are listed below in the current notation.

The variance of the input power to a subsystem is given by Eq. (12.3.5) of [2] versus Eqs. (4) and (9). Eq. (9) can actually be simplified [17] to better compare the two formulations:

$$\mathrm{Var}[P_{\mathrm{ran},k}] = P_{\mathrm{in},k}^2\left(\frac{\alpha_k}{\pi m_k'}\frac{1}{(1+B_k'/\pi)}\right)$$

versus

$$\mathrm{Var}[P_{\mathrm{ran},k}] \sim P_{\mathrm{in},k}^2\left(\frac{\alpha_k - 1}{\pi m_k'}\frac{1}{(1+B_k'/\pi)} + \frac{\ln(1+B_k'^2)}{(\pi m_k' B_k')^2}\right). \tag{B.1a,b}$$

The difference is due to adopting either a Poisson or a GOE description of the natural frequency statistics of an isolated subsystem. As detailed in Ref. [9], Eq. (B.1a) is expected to apply to systems with symmetry such as a bare rectangular simply supported plate, while Eq. (B.1b) would rather be valid for more random systems with no symmetry.

The variance of an off-diagonal term in the energy-power matrix is given by Eq. (12.3.7) of [2], where the energy-power matrix is assumed to be symmetric, versus Eqs. (5) and (9) where the energy-power matrix is not assumed to be symmetric:

$$\mathrm{Var}[C_{\mathrm{ran},ks}] = C_{ks}^2 \left(\frac{\alpha_k}{\pi m'_k} \frac{1}{(1 + B'_k/\pi)} \right) \left(\frac{\alpha_s}{\pi m'_s} \frac{1}{(1 + B'_s/\pi)} \right)$$

versus

$$\mathrm{Var}[C_{\mathrm{ran},ks}] \sim C_{ks}^2 \left(\frac{\alpha_{ks} - 1}{\pi m'_k} \frac{1}{(1 + B'_k/\pi)} + \frac{\ln(1 + B'^2_k)}{(\pi m'_k B'_k)^2} \right). \tag{B.2a,b}$$

The contribution to the energy variance from the coupling terms is given by the second term of Eq. (12.3.3) of [2] versus the second term of Eq. (3):

$$\sum_k \sum_s \left(C_{jk}^{-1} \hat{E}_s \right)^2 \mathrm{Var}[C_{\mathrm{ran},ks}] \text{ versus } \sum_k \sum_{s \neq k} \left((C_{jk}^{-1} - C_{js}^{-1}) \hat{E}_s \right)^2 \mathrm{Var}\left[C_{\mathrm{ran},ks} \right]. \tag{B.3a,b}$$

The difference arises from a power conservation constraint on the entries of the energy-power matrix, imposed by Eq. (30) of Ref. [3]. The variance of the diagonal terms of the energy-power matrix given by [2] is $\mathrm{Var}[C_{\mathrm{ran},kk}] = \sum_{j \neq k} \mathrm{Var}[C_{\mathrm{ran},jk}]$, and this term does not appear in the present formulation.

Appendix C. Confidence interval for the energy response

With the assumption that the statistical distribution of the subsystem energy is lognormal, the bounds of the confidence interval for a given confidence level CL ($0 < \mathrm{CL} < 1$) may be computed. The lognormal cumulative distribution function is given by

$$D(x) = \frac{1}{2} \left(1 + \mathrm{erf} \left[\frac{\ln(x) - M}{S\sqrt{2}} \right] \right), \tag{C.1}$$

where erf is the error function, and M and S are expressed in terms of the mean and variance of the energy as $\mathrm{E}[E] = \exp[M + S^2/2]$ and $\mathrm{Var}[E] = \mathrm{E}[E]^2(\exp[S^2] - 1)$. It follows that $S^2 = \ln(1 + \mathrm{Var}[E]/\mathrm{E}[E]^2)$.

Let E^- and E^+ denote the lower and upper bounds of the interval. Following Lyon's formulation [2,4], these bounds can be written as $E^- = \mathrm{E}[E]/\exp\{X\}$ and $E^+ = \mathrm{E}[E] \exp\{X\}$, where X can be obtained by solving $\mathrm{CL} = D(E^+) - D(E^-)$. This can be re-written as

$$\mathrm{CL} = \frac{1}{2} \left(\mathrm{erf} \left[\frac{S^2/2 + X}{S\sqrt{2}} \right] - \mathrm{erf} \left[\frac{S^2/2 - X}{S\sqrt{2}} \right] \right). \tag{C.2}$$

CL is a monotonically increasing function of X, from 0 to 1, with an asymptote of 1.

References

[1] M.S. Kompella, R.J. Bernhard, Measurement of the statistical variation of structural-acoustic characteristics of automotive vehicles, *Proceedings of the SAE Noise and Vibration Conference, Society of Automotive Engineers, Warrendale, USA*, 1993.
[2] R.H. Lyon, R.G. DeJong, *Theory and Application of Statistical Energy Analysis*, Butterworth-Heinemann, 1995.
[3] R.S. Langley, V. Cotoni, Response variance prediction in the statistical energy analysis of built-up systems, *Journal of the Acoustical Society of America* 115 (2004) 706–718.
[4] R.H. Lyon, Statistical analysis of power injection and response in structures and rooms, *Journal of the Acoustical Society of America* 45 (1969) 545–565.
[5] M.L. Mehta, *Random Matrices*, Academic Press, New York, 1991.
[6] J. Burkhardt, R.L. Weaver, The effect of decay rate variability on statistical response prediction in acoustical systems, *Journal of Sound and Vibration* 196 (1996) 147–164.
[7] R.L. Weaver, Spectral statistics in elastodynamics, *Journal of the Acoustical Society of America* 85 (1989) 1005–1013.
[8] P. Bertelsen, C. Ellegaard, E. Hugues, Distribution of eigenfrequencies for vibrating plates, *European Physical Journal B* 15 (2000) 87–96.
[9] R.S. Langley, A.W.M. Brown, The ensemble statistics of the energy of a random system subjected to harmonic excitation, *Journal of Sound and Vibration* 275 (2004) 823–846.
[10] R.S. Langley, A.W.M. Brown, The ensemble statistics of the band-averaged energy of a random system, *Journal of Sound and Vibration* 275 (2004) 847–857.
[11] X.L. Huang, C.J. Radcliffe, Probability distribution of statistical energy analysis model responses due to parameter randomness, *Journal of Vibration and Acoustics* 120 (1998) 641–647.
[12] R. Büssow, B.A.T. Petersson, Propagation of uncertainties in statistical energy analysis. *Proceeding of ICSV11, 5–8 July 2004, Saint Petersburg, Russia*, 2004, pp. 3307–3314.
[13] V. Cotoni, R.S. Langley, On the ensemble variance of energy of random plates under discrete and distributed loadings, *ESI R&D Internal Report*, 2004.
[14] M.R. Schroeder, Statistical parameters of the frequency response curves of large rooms, *Journal of the Audio Engineering Society* 35 (1987) 289–304.
[15] O.I. Lobkis, R.L. Weaver, I. Rozhkov, Power variances and decay curvature in a reverberant system, *Journal of Sound and Vibration* 237 (2000) 281–302.
[16] O.I. Lobkis, R.L. Weaver, Complex modal statistics in a reverberant dissipative body, *Journal of the Acoustical Society of America* 108 (2000) 1480–1485.
[17] M.R. Schroeder, Effect of frequency and space averaging on the transmission response of multimode media, *Journal of the Acoustical Society of America* 46 (1969) 277–283.
[18] AutoSEA2 2003 User's Guide, ESI Software, June 2003.
[19] F.J. Fahy, A.D. Mohammed, A study of uncertainty in applications of SEA to coupled beam and plate systems. I. Computational experiments, *Journal of Sound and Vibration* 158 (1992) 45–67.
[20] C.S. Manohar, A.J. Keane, Statistics of energy flows in spring-coupled one-dimensional systems, *Philosophical Transactions of the Royal Society: Physical Sciences and Engineering* 346 (1994) 525–542.